J Mater Sci (2015) 50:6730–6738
DOI 10.1007/s10853-015-9227-2

Superior strength of carbon steel with an ultrafine-grained microstructure and its enhanced thermal stability

M. V. Karavaeva[1] · S. K. Kiseleva[1] · A. V. Ganeev[1] · E. O. Protasova[1] · M. M. Ganiev[2] · L. A. Simonova[2] · R. Z. Valiev[1,3]

Received: 30 March 2015 / Accepted: 1 July 2015 / Published online: 8 July 2015

Abstract The paper presents the results of a study on the microstructure and mechanical properties of a medium-carbon steel (0.45 % C) processed by severe plastic deformation (SPD) via high-pressure torsion (HPT). Martensite quenching was first applied to the material, and then HPT processing was conducted at a temperature of 350 °C. As a result, a nanocomposite type microstructure is formed: an ultrafine-grained (UFG) ferrite matrix with fine cementite particles located predominantly at the boundaries of ferrite grains. The processed steel is characterized by a high-strength state, with an ultimate tensile strength over 2500 MPa. Special attention is given to analysis of the thermal stability of the microstructure and properties of the steel after HPT processing in comparison with quenching. It is shown that the thermal stability of the UFG structure produced by HPT is visibly higher than that of quenching-induced martensite. The origin of the enhanced strength and thermal stability of the UFG steel is discussed.

Introduction

Carbon steels belong to basic materials for modern materials science and engineering. This is associated with the fundamental nature of the studies of steels, as well as with their very wide practical application [1, 2]. It is no wonder that enhancement of the strength of steels remains one of the most topical problems in metallurgical engineering.

Quenching is the traditional method for strengthening of carbon steels. A martensite phase—a supersaturated solid solution of carbon in α-Fe, forms after quenching. The martensite is characterized by very high hardness, but has two considerable drawbacks: (1) extremely low tensile ductility (almost equal to zero) of steel with a martensite structure; (2) low thermal stability—decomposition of the supersaturated solid solution of martensite into a ferrite-cementite mixture during heating starts quickly and leads to a rapid decline in hardness and strength already after heating to 250 °C. In this connection, the problem of enhancement of the strength and ductility as well as thermal stability of low and medium alloyed carbon steels calls for new solutions.

Recently a lot of attention has been paid to the studies and developments of ultrafine-grained (UFG) metals and alloys, produced by the techniques of severe plastic deformation (SPD) [3–7]. Such UFG materials often demonstrate a unique set of mechanical properties, in particular high strength combined with a reasonable ductility [8, 9]. The yield strength of such alloys may exhibit a significant positive deviation from the values corresponding to the Hall–Petch relationship [4, 9]. The reason for such a deviation is the complexity of microstructures from SPD processing, which is especially typical of multiphase materials. For instance, during SPD processing of carbon steels, in addition to grain refinement, dissolution of cementite particles has been discovered [10, 11], as well as formation of segregations of carbon and cementite particles at the boundaries of nanocrystalline grains formed through deformation [12–16]. This provides an opportunity to realize a set of strengthening mechanisms in UFG carbon steels; in particular, in addition to the grain boundary

✉ M. V. Karavaeva
karma11@mail.ru

[1] Ufa State Aviation Technical University, Ufa, Russia

[2] Kazan Federal University, Kazan, Russia

[3] Saint PetersburgState University, Saint Petersburg, Russia

strengthening mechanism, also the dislocation strengthening, precipitate strengthening and solid solution strengthening mechanisms [12, 15], as well as the new strengthening mechanism associated with solute segregation at grain boundaries [15, 16], make their contributions. Such a superposition of the strengthening mechanisms allows to enhance considerably the strength of carbon steels [12, 17–20].

It has been shown recently that the use of the initial martensite structure of low-carbon steels allows to obtain a UFG structure at lower plastic strains than during deformation of an initial ferrite-pearlite microstructure [21–23].

In the present work, this approach was used during the processing of a medium-carbon steel at an elevated temperature in order to produce a two-phase UFG structure with enhanced strength, ductility, and thermal stability.

Experimental

Commercial medium-carbon steel C45 (DIN C45) (0.45 % C; 0.27 % Si; 0.65 % Mn) of a Russian manufacturer was used in this study. Before SPD processing the samples were water-quenched with preliminary heating at 800 °C for 1 h.

SPD processing was conducted by high-pressure torsion (HPT) at an elevated temperature of 350 °C with a number of turns $N = 5$ and a pressure of $P = 5$ GPa [13, 14]. The processing was performed on disk samples with a diameter of 10 mm and a thickness of 0.2 mm.

The microstructure was studied using a JEOL® JSM 6390 scanning electron microscope (SEM). The TEM studies of the samples were performed on a JEOL® JEM-2100 transmission electron microscope at an accelerating voltage of 200 kV. The TEM samples were cut out from the the half radius of the deformed disks and subjected to electropolishing with electrolyte (90 vol% ethanol + 10 vol% perchloric acid).

The dislocation density ρ_{XRD} was assessed according to formula (1) [24]:

$$\rho_{XRD} = \frac{2\sqrt{3}\langle\varepsilon^2\rangle^{1/2}}{bd_{XRD}}, \quad (1)$$

where $\langle\varepsilon^2\rangle^{1/2}$ is the level of elastic microdistortions of a crystalline lattice; b is the Burgers vector; d_{XRD} is the coherent scattering domain size.

The parameters values in formula (1) and the lattice parameter were determined by an X-ray diffraction technique on a DRON 4 M diffractometer using C_oK_α—radiation with a graphite monochromator on a diffracted beam from the positions of the three basic maxima of the X-ray diffraction pattern. The range of 2θ angles was 40°–140° with a step of 0.1° and an exposure time of 20 s.

The microhardness was determined using a MICRO-MET 5101 microhardness tester with a load of 0.1 kg for 10 s. Mechanical tests were performed on a specialized machine for precision testing of small-sized samples with a gage length of 2 mm and a thickness of 0.1 mm [25]. Tensile specimens were cut in a way so that the gage section was located approximately at the half radius of the disk center.

Results

A lath martensite [26] structure was produced after quenching from the austenite region (Fig. 1a, b).

The average size of the packets of martensite plates in the as-quenched microstructure was 8 ± 0.5 μm, the average width of the plates was 0.3 ± 0.1 μm. The lattice parameter value of C45 after quenching was $a = 2.8680 \pm 0.00025$ Å, which exceeded the lattice parameter of α-iron ($a = 2.86645$ Å), indicating supersaturation of α-iron with carbon in the as-quenched state [27].

Besides, the boundaries of prior-austenite grains can be seen clearly in the martensite structure (Fig. 1a) [22, 26, 27]. The average austenite grain size was 18 ± 0.5 μm. The misorientations between martensite plates within a block are low-angle [26, 27], each martensite plate is a single crystal. A developed dislocation substructure is observed in the volume of martensite crystals (Fig. 1b), the occurrence of which is determined by the rate and volume effect of martensitic transformation [26, 27].

The microhardness of the steel after quenching is essentially higher than that in the initial state—over 8000 MPa (Fig. 2). The microhardness value of 3030 ± 50 MPa of the initial steel is shown in Fig. 2 for comparison.

The mechanical properties of the steel are given in Table 1.

The as-quenched martensitic state of steel was characterized by high strength accompanied by brittle fracture with a low ductility (Fig. 3; Table 1) [26, 27].

Tempering of the steel occurs during heating of the steel for 5 min prior to HPT processing, which produces thin plate-like cementite particles with a thickness of 10–20 nm and a length of up to 400 nm in the martensite plates (Fig. 1d).

As a result of holding at an elevated temperature prior to HPT processing, the microhardness decreases practically twice to 5000 MPa (Fig. 2). However, this value of microhardness is higher than that in the initial ferrite-pearlite state (Fig. 2), which may be associated with an incomplete decomposition of the supersaturated solid solution. This is confirmed by the results of X-ray structural analysis: the matrix lattice parameter value after heating achieved

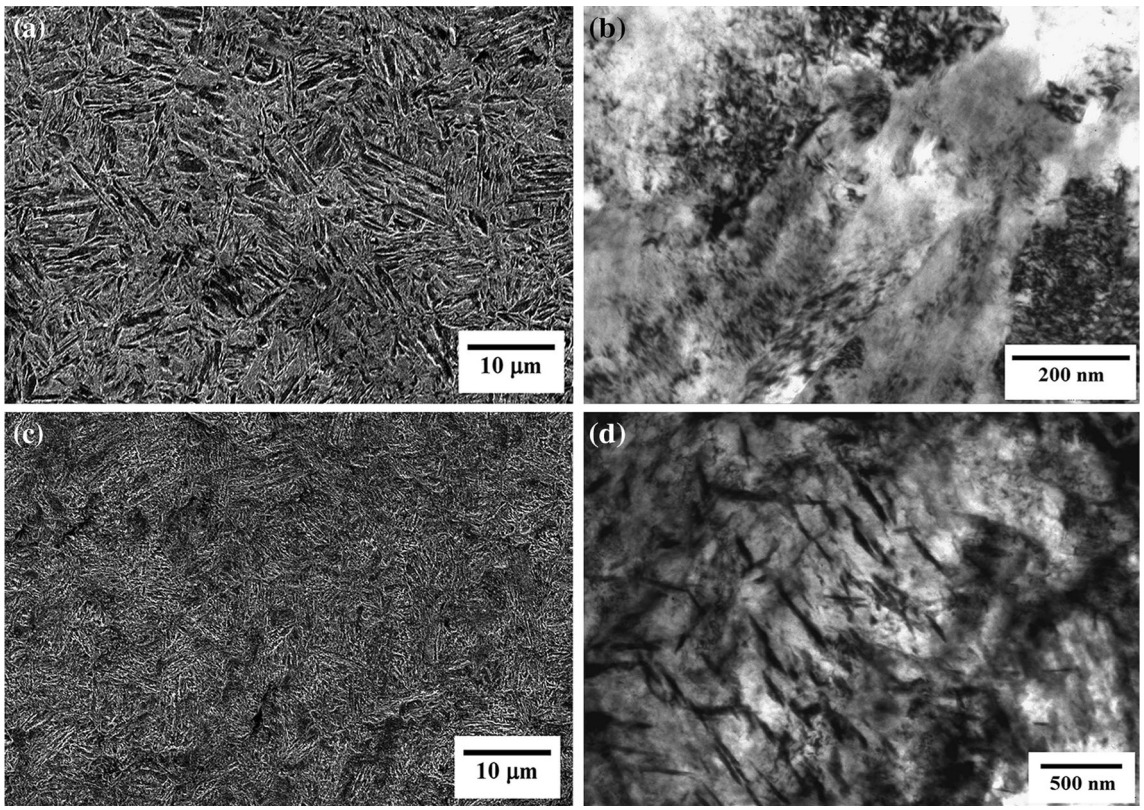

Fig. 1 Microstructure of C45 before HPT processing: **a**, **b** as-quenched; **c, d** after quenching and 5-min holding at $T = 350$ °C. **a**, **c** SEM; **b**, **d** TEM

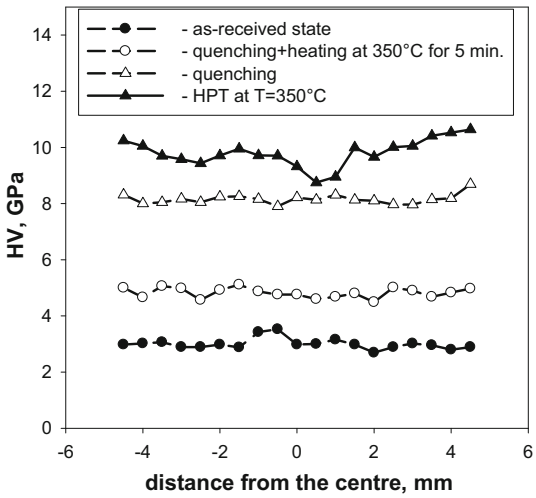

Fig. 2 Microhardness of C45 after various types of treatment

2.867 ± 0.00013 Å, which is lower than that recorded after quenching ($a = 2.868 \pm 0.00025$ Å), but higher than that for pure iron ($a = 2.86645$ Å). The steel strength also decreases almost twice, as compared to the quenched state, while the ductility grows more than ten times (Table 1).

The TEM studies demonstrated considerable microstructure refinement as a result of HPT (Fig. 4a, b). The average grain size calculated from the dark-field images (Fig. 4c) is 120 ± 50 nm. The SAED pattern demonstrates numerous spots positioned along circles, which is an evidence of high-angle misorientations and ultrafine grains. However, some spots have noticeable azimuthal blurring, which assumes low-angle boundaries and high internal stresses (Fig. 4a).

The lamellar cementite precipitates that formed during tempering caused by heating prior to straining (Fig. 1d) are not observed after straining. Highly dispersed spherical particles of cementite can be seen, which are located predominantly at the α-phase grain boundaries (Fig. 4b, d). The average particle size is 15 ± 5 nm. The lattice parameter value of ferrite after HPT processing reaches 2.867 ± 0.00016 Å, and consequently, part of the carbon is preserved in the solid solution, thus providing its supersaturation to a certain extent, as compared with the equilibrium state.

The microhardness of C45 after HPT processing varies from the minimum value of 9320 MPa in the sample center to the maximum value of 10638 MPa on the periphery (Fig. 2), the average value is 9810 ± 490 MPa. The microhardness

Table 1 Mechanical properties of C45 in various conditions

Condition	σ_{Ult} (MPa)	σ_y (MPa)	δ (%)	HV (GPa)
As-received state (Initial rod)	863	770	7	3 ± 0.2
T = 800 °C, 60 min, water quenching	2192	1998	0.4	8.15 ± 0.17
T = 800 °C, 60 min, water quenching + heating, T = 350 °C, 5 min	1665	1350	12	4.82 ± 0.18
T = 800 °C, 60 min, water quenching + HPT, T = 350 °C, 5 turns, 5 GPa, 1 rpm	2649	2397	3	9.81 ± 0.49

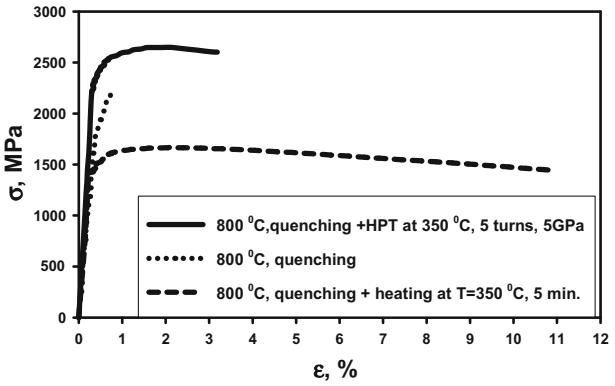

Fig. 3 Engineering stress–strain curves of C45 after various types of treatment

values through the section are higher than those in the quenched steel and are characterized by a rather uniform distribution along the diameter (Fig. 2). This allows assuming that the microstructure is uniform in the sample volume.

After HPT processing, strength enhancement is observed, in comparison with the state by the moment of the HPT processing start (after quenching and holding at a temperature of 350 °C for 5 min), as well as in comparison with the as-quenched martensite state (Fig. 3). The ultimate tensile strength is over 2600 MPa which is a record value for medium-carbon steel. The yield strength and hardness values increase as well. At the same time, the total elongation is about 3 %, which is also higher than the value obtained during tension of the quenched steel (see Table 1).

The thermal stability of properties was estimated from the variation of the microhardness after heating of the steel. Figure 5 displays the results.

As a result of heating to temperatures up to 350 °C with a holding time up to 5 h, the microhardness is stable (Fig. 5a), at the heating temperature of 400 °C a decline in microhardness is observed after holding for 60 min; and during up to 5 h the microhardness value is retained at a high level, up to 8000 MPa (Fig. 5b), i.e., practically up to the values typical for the quenched steel. As a result of annealing at a temperature of 450 °C, the microhardness falls noticeably already after 15 min of holding, and with increasing annealing time, the microhardness monotonously decreases to around 7400 ± 350 MPa after holding for 5 h (Fig. 5c). Therefore, it can be concluded that at a short-term holding for 15 min the microhardness is stable until 400 °C; at long-term holding (up to 300 min), the microhardness is stable until 350 °C. In spite of reduction in the microhardness after heating to temperatures of 400–450 °C, the microhardness value is retained at a high level, around 7000 MPa.

Other dependencies are observed during heating of the quenched steel (Fig. 5). At any temperature of heating, the sharpest decline in microhardness is observed already after the first 15 min, then as the time and temperature of heating increase, the microhardness monotonously decreases at a lower speed. The microhardness values after heating in the whole range of the investigated temperatures of the as-quenched steel have become significantly lower than those of the UFG steel processed by HPT. Thus, it follows from Fig. 5 that C45 with a UFG microstructure processed by SPD demonstrates a significantly higher strength and thermal stability than the quenched steel with a martensitic microstructure.

After annealing at temperatures of 300 and 350 °C, the microstructure observed after the HPT processing remains practically unchanged. Correspondingly, no noticeable change in microhardness takes place (Fig. 5a). First recrystallized grains appear in the steel structure after annealing at a temperature of 400 °C. This is accompanied by a decline in microhardness, as illustrated in Fig. 5b.

The steel microstructure after heating at temperatures of 450 °C for 60 min is displayed in Fig. 6.

After annealing at a temperature of 450 °C, the microstructure changes essentially as a result of recrystallization. The structure represents a ferritic matrix and cementite particles (Fig. 6a, b) situated predominantly at the boundaries of ferrite grains. The grain size has increased to 250 ± 50 nm, the size of cementite particles grows to 30–50 nm as a result of coagulation.

Discussion

Quenching is a well-known conventional method for strengthening of carbon steels, leading to formation of a martensite structure which demonstrates very high-strength characteristics—a yield strength above 2000 MPa (Fig. 3).

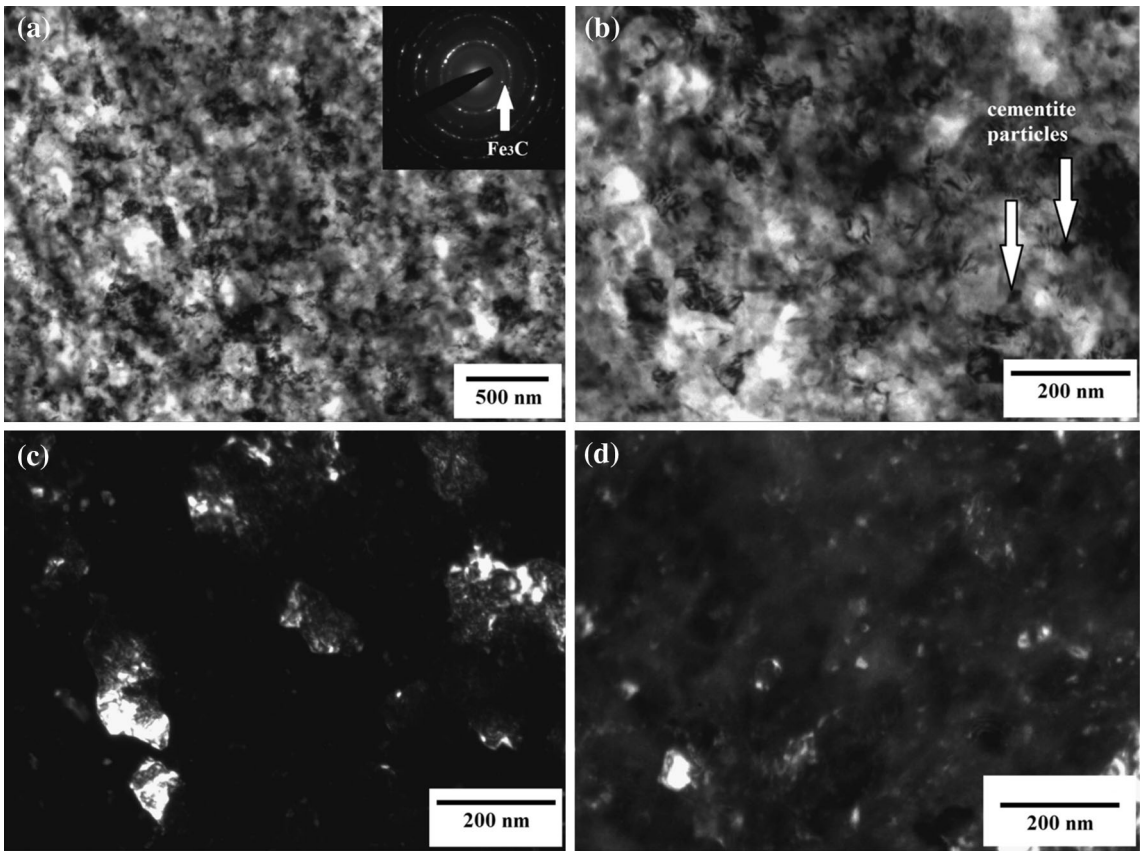

Fig. 4 Microstructure of C45 processed by high-pressure torsion (TEM): **a**, **b** bright-field images; **c**, **d** dark-field images; **c** in the ferrite spot; **d** in the cementite spot, indicated by an *arrow* in the insert in **a**. In **b** the *arrows* indicate cementite particles at grain boundaries

Martensite is a heavily supersaturated solid solution of carbon in α-iron, and it is characterized by a complex hierarchical structure [22, 26]. Besides, a high-dislocation density is observed in martensite plates. Therefore, high strength of martensite is caused by simultaneous action of several strengthening mechanisms: solid solution, dislocation, and grain boundary strengthening. Let us evaluate the contributions of these mechanisms to the yield strength of C45 in the first approximation of linear additivity [28, 29]:

$$\sigma_y = \sigma_0 + \Delta\sigma_{GB} + \Delta\sigma_{SS} + \Delta\sigma_{Or} + \Delta\sigma_D, \quad (2)$$

where σ_0 is the friction stress of the α-iron lattice; $\Delta\sigma_{GB}$ is grain boundary strengthening; $\Delta\sigma_{SS}$ is solid solution strengthening; $\Delta\sigma_{Or}$ is precipitation hardening; $\Delta\sigma_D$ is dislocation strengthening.

The linear additivity principle of strengthening mechanisms is successfully applied to evaluate the yield stress of different ultrafine-grained materials [15, 28–31], often demonstrating good agreement with experimental data.

The friction stress of the α-iron lattice (σ_0) is defined by the Peierls-Nabarro stress:

$$\sigma_0 = 2 \times 10^{-4} G, \quad (3)$$

where $G = 78\,000$ MPa is the shear elastic modulus of ferrite.

Grain boundary strengthening ($\Delta\sigma_{GB}$) can be determined by the mean grain size in accordance with the Hall–Petch equation:

$$\Delta\sigma_{GB} = K_y d^{-1/2}, \quad (4)$$

where K_y is the coefficient characterizing the contribution of grain boundaries to strengthening; d is the grain size.

The packet size of martensite plates (d = 8 μm) was used as the grain size for the martensite structure during the calculation [26].

The value of K_y for carbon steels, according to various published data [28, 29, 32–36], varies in a very broad range: from 0.13 MPa/m$^{1/2}$ in commercially pure iron practically without any impurities [31] to 0.70 MPa/m$^{1/2}$ in tempered steel [32]. The value of K_y is influenced by the content of alloying elements, in particular carbon [36], the degree of plastic strain (in other words, dislocation density) [35] and other parameters. However, the value of K_y as an indicator of the impediment of dislocations in front of a grain boundary cannot depend on the

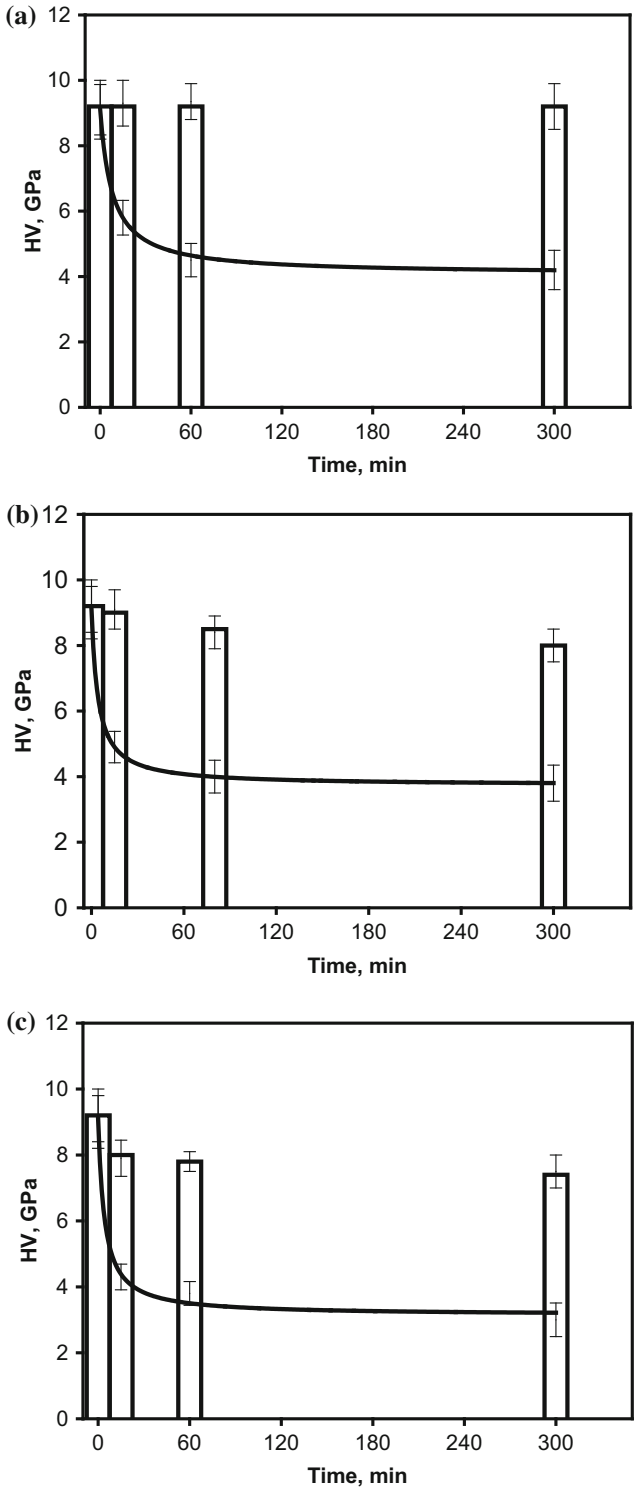

Fig. 5 Variation of the microhardness of C45 after heating to a temperature of: **a** 350 °C; **b** 400 °C; **c** 450 °C. The *column* represents steel with a UFG microstructure processed by HPT, the line represents steel in the as-quenched state

intragranular structural state (dislocation density, alloying, and etc.), unlike the coefficient of proportionality between the yield strength σ_y and the grain size $d^{-1/2}$. In case the yield strength is viewed as a superposition of the contributions of different strengthening mechanisms (2), intragranular strengthening factors are taken beyond the scope of the Hall–Petch model (4) and calculated separately. Consequently, when considering the contribution of grain boundaries to strengthening on its own as the value of K_y, it is necessary to accept the value typical for unalloyed undeformed ferrite.

In the present work, the following value is accepted: $K_y = 0.4$ MPa m$^{-1/2}$ [32, 33].

Solid solution strengthening ($\Delta\sigma_{SS}$) is defined by the content of the alloying element and its strengthening action:

$$\Delta\sigma_{SS} = k \cdot c \tag{5}$$

where k is the strengthening coefficient for ferrite, representing an increment in the yield strength during dissolution of 1 % (wt) alloying element in it (for carbon $k = 4670$ MPa/ % [28]); c is the concentration of the alloying element in % (wt).

For the first approximation calculation, the carbon content in the solid solution is accepted as 0.4 % for the C45 martensite.

Precipitation hardening ($\Delta\sigma_{Or}$) is calculated in accordance with Orowan's formula:

$$\Delta\sigma_{\mathrm{Or}} = 0.85M\frac{Gb}{2\pi(\lambda - \bar{D})}\Phi\ln\left(\frac{\lambda - \bar{D}}{2b}\right), \tag{6}$$

where b is the Burgers vector of dislocations (for ferrite b/2 <111> is 0.25 nm); λ is the average distance between the centers of the particles; $\overline{D}$ is the average particle size; Φ is the coefficient characterizing the type of dislocations interacting with the particles: for steel $\Phi = 1.25$; for α-iron $M = 2.75$; 0.85 is the static coefficient [28].

It can be accepted in the first approximation that there are no dispersed particles in the steel martensite, therefore this component will not be taken into account in the martensite yield strength calculation.

Dislocation strengthening ($\Delta\sigma_D$) is defined by the relationship [28]:

$$\Delta\sigma_D = \alpha MbG\rho^{1/2}, \tag{7}$$

where α is the coefficient depending on the character of dislocation interaction in the course of work hardening; M is the orientation multiplier: for α-iron $M = 2.75$, and the product $\alpha M \approx 0.5$; $b = 0.25$ nm is the Burgers vector; ρ is the dislocation density.

The dislocation density determined by the X-ray diffraction method for the martensite was $\rho = 1.5 \times 10^{13}$ m^{-2}.

The calculation results are listed in Table 2.

One can see from Table 2, the calculated value of the yield strength in the quenched state of steel is close to the

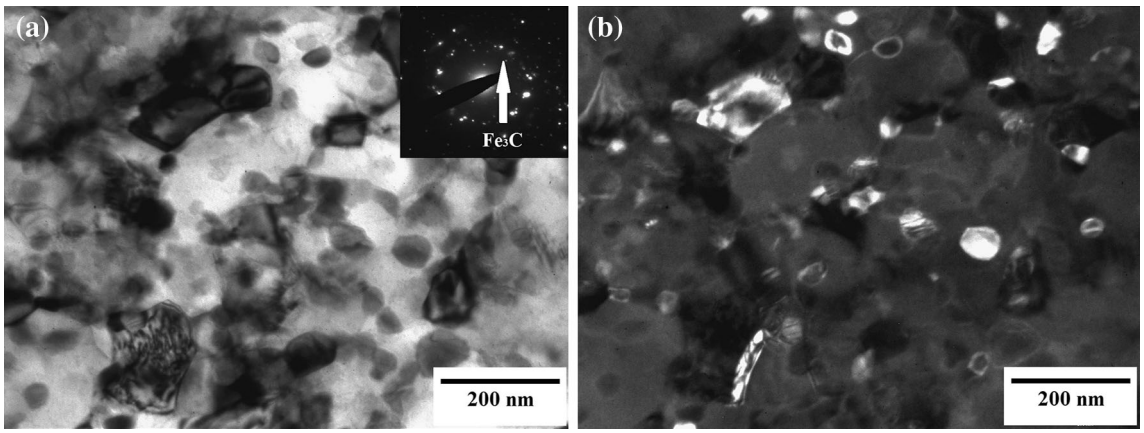

Fig. 6 The UFG microstructure of the C45 processed by HPT after heating to a temperature of 450 °C. **a** bright field; **b** dark field in the cementite spot indicated by an *arrow* in the insert in **a**

Table 2 Calculated values of the contributions of different strengthening mechanisms to the yield strength of C45

Condition	σ_0 (MPa)	$\Delta\sigma_{SS}$ (MPa)	$\Delta\sigma_{GB}$ (MPa)	$\Delta\sigma_D$ (MPa)	$\sigma_Y = \sum_{i=1}^{n} \sigma_i$ (MPa)	σ_Y (MPa) experimental value
$T = 800$ °C—60 min, water quenching	16	1868 (90 %)	141 (7 %)	39 (3 %)	2064	1998
T = 800 °C—60 min, water quenching + HPT, $T = 350$ °C, $N = 5$, 5 GPa	16	467 (27 %)	1154 (67 %)	91 (6 %)	1728	2397

experimental one. This confirms adequacy of the chosen model of the linear additivity of strengthening mechanisms for the assessment of the steel yield strength. It can be seen also that the main contribution to the strengthening of quench-induced martensite (about 90 %) is made by the formation of a supersaturated solid solution.

An alternative way of strengthening is grain refinement by severe plastic deformation. SPD processing enables forming an ultrafine-grained microstructure of the nanocomposite type in the steel: a ferrite matrix with a grain size of 120 ± 50 nm and uniformly located, predominantly at grain boundaries, highly dispersed spherical particles of cementite with a size of 15 nm. The formation of a nanocomposite structure during HPT processing at an elevated temperature is the consequence of two simultaneous processes—grain refinement resulting from severe plastic deformation and dynamic tempering of the initial martensite structure. Notably, absence of clear images of grain boundaries in the photographs of microstructure made using TEM (Fig. 4) is indicative of high non-equilibrium grain boundaries with strain-distorted structure.

The structure produced by SPD demonstrates a high level of strength: the yield strength is around 2400 MPa, which is a record value for C45. Such a high value as well as for martensite can be the result of the simultaneous action of several strengthening mechanisms. In the first place, it is the grain boundary strengthening in accordance with the Hall–Petch equation. In addition, dislocation strengthening, precipitation hardening and solid solution strengthening can also lead to an increase in the yield strength.

Let us calculate the contributions of the strengthening mechanisms in the steel processed by SPD in accordance with the same formulas (3)–(7) that were used when calculating the yield strength of the martensite. The contribution of the precipitation mechanism is not determined, as the cementite particles are located predominantly at grain boundaries and, consequently, they do not impede the movement of dislocations. In the calculations, the same values of the coefficients are used as in the case of the martensite structure. The grain size in the steel processed by HPT is $d = 120$ nm. It is difficult to determine precisely the carbon content in the solid solution, and the value $C = 0.1$ % was accepted for the calculations based on the value of the lattice parameter. The dislocation density determined from the results of X-ray structural studies reaches $\rho = 7.5 \times 10^{13}$ m^{-2}.

The results of the calculations are listed in Table 2. It can be seen from Table 2 that a principally different distribution of the contributions of different mechanisms to yield strength is typical of the UFG steel. In this case, grain boundary strengthening has the greatest significance—67 %, and the solid solution component also makes

a considerable contribution—27 %. The calculated value of the yield strength for the deformed steel has turned out to be 27 % lower than the experimental value. The underestimation of the yield strength value in the calculation can be associated with two reasons: first, a higher actual content of carbon in the solid solution and a certain fraction of cementite particles in the grain body; second, the action of a new strengthening mechanism not taken into account in (2). Such a strengthening mechanism could be associated with formation of carbon segregations at grain boundaries, observed recently in carbon steels produced by HPT [12, 15, 37]. It has been shown [16] that segregations can significantly impede dislocation nucleation from grain boundaries and cause additional strengthening.

It follows from the calculation results given in Table 2 that the high strength of the martensite is related, in the first place, to solid solution strengthening, while the high strength of the steel with a nanocrystalline structure is related to grain boundary strengthening.

These differences in strengthening mechanisms make influence essentially on a higher thermal stability of the structure and properties of the steel nanostructured by SPD.

Processes lead to reduction of the free energy take place during heating of the steel. They are precipitation of carbon from the matrix with formation of cementite particles, recovery, and recrystallization.

Let us compare the action of these processes during the annealing of the steel with martensite and nanocrystalline structures.

The decomposition of the supersaturated solid solution of martensite is connected with the diffusion of carbon in the ferrite lattice. This process runs even at room temperature and significantly accelerates during heating [26, 27]. As was shown above, the main contribution to the strengthening of the martensite is made by the solid-solution component, therefore during the decomposition of the martensite, softening is observed: the microhardness and the yield strength decrease 1.5 times already after holding for 5 min at a temperature of 350 °C prior to SPD processing (Figs. 2, 5; Table 1).

As known, the recrystallization process is associated with the self-diffusion of atoms of iron. Recrystallization is observed in the martensite structure at temperatures higher than the temperatures studied in this paper. A recrystallized microstructure forms in the nanocrystalline structure of the steel at a temperature of 450 °C (Fig. 6). This confirms the conclusions made above that the main strengthening mechanism in the nanocrystalline steel is the grain boundary one: the two-fold growth of the grain size as a result of recrystallization leads to a considerable softening, which was observed during our experiment (Fig. 5c).

The performed investigation has demonstrated that the thermal stability of the high-strength state of steel 45 is determined by the active strengthening mechanisms. The latter, in their turn, determine the processes taking place during heating of the steel and, consequently, the kinetics of softening and the thermal stability.

Conclusions

1. Severe plastic deformation at an elevated temperature of C45 with the initial martensite microstructure can be viewed as an effective approach to produce the high-strength state, alternative to quenching. Its implementation leads to the formation of ultrafine-grained ferrite matrix with highly dispersed carbides located predominantly at grain boundaries. This steel exhibits record values of strength characteristics: a yield strength of about 2400 MPa, an ultimate tensile strength above 2600 MPa.
2. In contrast to the martensite, in which the main strengthening factor is supersaturated solid-solution formation, it is grain boundary strengthening that is responsible for the high-strength state of the ultrafine-grained steel.
3. The thermal stability of the microstructure and properties of the steel with an ultrafine-grained microstructure exceeds the thermal stability of the martensite, which is related to principally different softening mechanisms taking place during heating. The main softening factor for the martensite is the decomposition of supersaturated solid solution, associated with carbon diffusion. For the UFG structure, softening is associated with recrystallization, i.e., self-diffusion of atoms of iron, which proceeds at higher temperatures.

Acknowledgements M.V. Karavaeva gratefully acknowledges the financial support from the RFBR, project No.14-08-90429. M. M. Ganiev and L. A. Simonova gratefully acknowledge the funding through the Russian Government Program of Competitive Growth of Kazan Federal University. R.Z. Valiev gratefully acknowledges the Russian Federal Ministry for Education and Science (through RZV Grant No. 14.B25.31.0017). A.V.Ganeev is greatly acknowledges of A.von Humboldt foundation (Group Linkage Project Fokoop —DEU/1052606).

References

1. Whang SH (2011) Nanostructured metals and alloys. Processing, microstructure, mechanical properties and applications. Woodhead Published Limited, Cambridge
2. Okitsu Y, Takata N, Tsuji N (2009) A new route of fabricate ultrafine-grained structures in carbon steels without severe plastic deformation. Scripta Materialia 60:76–79
3. Valiev RZ, Zhilyaev AP, Langdon TG (2013) Bulk nanostructured materials: fundamentals and applications. Wiley, Hoboken

4. Valiev RZ, Islamgaliev RK, Alexandrov IV (2000) Bulk nanostructured materials from severe plastic deformation. Prog Mater Sci 45(2):102–189
5. Valiev RZ, Alexandrov IV (2007) Bulk nanostructured metallic materials. Akademkniga, Moscow (in Russian)
6. Haddad M, Ivanisenko Yu, Courtois-Manara E et al (2015) In-Situ tensile test of high strength nanocrystalline bainitic steel. Mater Sci Eng, A 620:30–35
7. Valiev RZ (2004) Nanostructuring of metals by severe plastic deformation for advanced properties. Nat Mater 3:511–516
8. Tsuji N, Kamikava N, Ueji R et al (2008) Managing both strength and ductility in ultrafine grained steels. ISIJ Int 48:1114–1121
9. Tsuji N, Ito Y, Saito Y et al (2002) Strength and ductility of ultra grained aluminum and iron produced by ARB and annealing. Scripta Mat 47:893–899
10. Ivanisenko Yu, Lojkowski W, Valiev RZ et al (2003) The mechanism of formation of nanostructure and dissolution of cementite in a pearlitic steel during high pressure torsion. Acta Mater 51:5555–5570
11. Ivanisenko Yu, Wunderlich RK, Valiev RZ et al (2003) Annealing behavior of nanostructured carbon steel produced by severe plastic deformation. Scr Mater 49:947–952
12. Ganeev AV, Karavaeva MV, Sauvage X et al (2014) On the nature of high-strength state of carbon steel produced by severe plastic deformation. IOP Conf. Series. Mate Sci Eng 63:012128
13. Karavaeva MV, Kiseleva SK, Abramova MM, Ganeev AV, Valiev RZ (2014) Microstructure, properties, and failure characteristics of medium-carbon steel subjected to severe plastic deformation, IOP Conf Ser 63(2014):012056
14. Karavaeva MV, Nurieva SK, Zaripov NG et al (2012) Microstructure and mechanical properties of medium-carbon steel subjected to severe plastic deformation. Met Sci Heat Treat 54:155–159
15. Abramova MM, Enikeev NA, Valiev RZ et al (2014) Grain boundary segregation induced strengthening of an ultrafine-grained austenitic stainless steel. Mat. Letters 136:349–352
16. Valiev RZ, Enikeev NA, Murashkin M Yu et al (2010) On the origin of the extremely high strength of ultrafine-grained Al alloys produced by severe plastic deformation. Scr. Mater 63: 949–952
17. Wang J, Xu C, Wang Y et al (2003) Microstructure and properties of a low carbon steel after equal channel angular pressing. In: Zehetbauer MJ, Valiev RZ (eds) Nanomaterials by severe plastic deformation. J WileyVCH, Weinheim, pp 829–834
18. Zrnik J, Pippan R, Scheriau S et al (2010) Microstructure and mechanical properties of UFG medium carbon steel processed by HTP at increased temperature. J Mater Sci 45:4822–4826
19. Zrnik J, Dobatkin S, Stejskal O et al (2007) Deformation behaviour and ultrafine graned structure development in steels with different carbon content subjected to severe plastic deformation. Key Eng. Mat. 345–346:45–48
20. Valiev RZ, Enikeev NA, Langdon TG (2011) Towards superstrength of nanostructured metals and alloys, produced by SPD. Kovove Mater 49:1–9
21. Tsuji N, Ueji R, Minamino Y et al (2002) A new and simple process to obtain nano-structured bulk low-carbon steel with superior mechanical property. Scripta Mater 46:305–310
22. Tsuji N (2010) New routes for fabricating ultrafine grained microstructures in bulky steels without very high strains. Adv Eng Mater 12:701–707
23. Ueji R, Tsuji N, Minamino Y et al (2002) Ultragrain refinement of plain low carbon steel by cold-rolling and annealing of martensite. Acta Mater 50:4177–4189
24. Williamson G, Smallman R III (1956) Dislocation densities in some annealed and cold-worked metals from measurements on the X-ray Debye-Scherrer spectrum. Philos Mag 1:34–45
25. Kurmanaeva L, Ivanisenko Yu, Markmann J, Kübel C, Chuvilin A, Doyle S, Valiev RZ, Fecht H-J (2010) Grain refinement and mechanical properties in ultrafine grained Pd and Pd–Ag alloys produced by HPT. Mater Sci Eng A 527:1776–1783
26. Nishiyama Z (1978) Martensitic transformations. Academic Press, New York
27. Askeland D., Wrigth W. (2013) Essentials of materials science & engineering. SI Edition, Cengage Learning Stamford, USA
28. Goldstein MI, Litvinov VS, Bronfin BM (1986) Metal physics of the high-strength state. Metallurgiya, Moscow **(in Russian)**
29. Halfa H (2014) Recent Trends in Producing Ultrafine Grained Steels. J Miner Mater Character Eng. doi:10.4236/jmmce.2014.25047
30. Kozlov EV, Zhdanov AN, Popova NA, Pekarskaya EE, Koneva NA (2004) Subgrain structure and internal stress fields in UFG materials: problem of Hall-Petch relation. Mat Sci Eng A 387–389:789–794
31. Kamikawa N (2014) Y. ABE, G. Miyamoto, Y. Funakawa and T. Furuhara Tensile behavior of Ti, Mo-added low carbon steels with interphase precipitation. ISIJ Int 54(1):212–221
32. Takaki S (2010) Review on the Hall-Petch relation in ferritic steel. Mat Sci Forum 654–656:11–16
33. Malow TR, Koch CC (1998) Mechanical properties, ductility, and grain size of nanocrystalline iron produced by mechanical attrition. Met Mater Trans A 29:2285–2295
34. Nam WJ, Bae CM, Lee CS (2002) Effect of carbon content on the Hall-Petch parameter in cold drawn pearlitic steel wires. J Mat Sci 37:2243–2249
35. Armstrong RW (2013) Hall-Petch analysis of dislocation pileups in thin material layers and in nanopolycrystals. J Mater Res 28:1792–1798
36. Takaki S (2010) Effect of carbon and nitrogen on the Hall–Petch coefficient of ferritic iron. Mater Sci Forum 638–642:173–186
37. Sauvage X, Ganeev A, Ivanisenko Yu et al (2012) Grain boundary segregation in ufg alloys processed by severe plastic deformation. Adv Eng Mater. doi:10.1002/adem.201200060